Pure Appl. Geophys. 179 (2022), 1159–1172

https://doi.org/10.1007/s00024-022-02989-y

Pure and Applied Geophysics

S-Wave Attenuation Due to Fluid Acceleration

Guangquan Li,[1] Yonggang Liu,[2] and Shiwei Liu[1]

Abstract—At high frequency, the time scale is very short and acceleration becomes important. There must be a pressure difference in the main pores to drive fluid acceleration, which as a side effect is capable of inducing a reverse squirt in the throat connecting two pores. Based on such a mechanism, we develop a novel model of an S wave in fluid-saturated rock, which yields phase velocity (V_s) and the quality factor (Q_s) as functions of frequency. Applications of the new model to Berea sandstone and Boise sandstone yield throat permeability. The second porosity represented by throats appears to be 5% of the total porosity. Nonetheless, Q_s is predicted as 10^6 at a frequency of 10 Hz, far higher than seismic Q_s measured in the field. This may be because groundwater has softened the skeleton of sedimentary rocks and/or because internal reflections at multiple lithological interfaces attenuate seismic waves.

Keywords: S wave, quality factor, fluid acceleration, reverse squirt, throats.

List of Symbols

a	Length of main pore
b	Length of throat
c_s	S-wave velocity in undrained rock ($c_s = \sqrt{\frac{G}{\rho}}$)
c_{s0}	S-wave velocity of skeleton ($c_{s0} = \sqrt{\frac{G}{\rho_s}}$)
f	Frequency
G	Shear modulus of skeleton
k	Wavenumber
k_D	Darcy permeability
k_1	Local permeability of S wave in main pore
k_2	Local permeability of S wave in throat
P_{p1}	Fluid pressure in main pore
P_{p2}	Fluid pressure in throat
q_1	Darcy flux rate in main pore
q_2	Darcy flux rate in throat
Q_E	Quality factor of FOM
Q_p	Quality factor of P wave
Q_s	Quality factor of S wave
t	Time
u	Shear displacement
v	Lagrangian velocity of solid
V_s	S-wave velocity
x	Direction of Lagrangian motion
y	S-wave direction
ϕ	Total porosity
ϕ_1	Local porosity in main pore
ϕ_2	Local porosity in throat
μ	Fluid dynamic viscosity
ω	Angular frequency
ω_C	Characteristic angular frequency
Ω	Dimensionless angular frequency
ρ	Total density ($\rho = \rho_s + \phi\rho_f$)
ρ_f	Fluid density
ρ_s	Skeleton density

[1] Department of Geophysics, Yunnan University, Kunming 650504, Yunnan, China. E-mail: liguangquan@ynu.edu.cn; liu666sw@163.com

[2] Institute of Geochemistry, Chinese Academy of Sciences, 99 West Lincheng Road, Guiyang 550081, Guizhou, China. E-mail: liuyonggang@vip.gyig.ac.cn

1. Introduction

Porous rocks are often saturated with groundwater, oil or gas. Fluid is different from the skeleton (the voided solid) in two respects: (1) fluid can flow and reach a great distance, whereas the skeleton cannot; (2) for a static fluid, the pressure is the same in different directions (Kundu, 1990), whereas a static skeleton allows for three different principle stresses (Jaeger et al., 2007).

There is little controversy regarding the momentum equation of rock as a fluid–solid aggregate. However, the debate on the momentum equation of a fluid has not yet been resolved. Various models have proposed different fluid momentum equations. The simplest one is undrained rock (permeability is

assumed to vanish and fluid velocity is precisely the same as solid velocity). Consequently, viscous stress between solid and fluid vanishes. Generally, fluid and solid have different velocities, such that there is a viscous stress between them. The ability to quantify the viscous stress is the key to modeling acoustic waves in fluid-saturated rocks.

Darcy's law is a fluid momentum equation widely used in hydrogeology (Bear, 1972). Originally, Darcy's law was found from seepage experiments. It was later recognized that the law has a theoretical proof from the Navier–Stokes equation in fluid mechanics (Bear, 1972; Kundu, 1990). The law is only applicable at very low frequency, and not for high frequency (when fluid acceleration is large). According to Darcy's law, fluid viscosity (μ) divided by the Darcy permeability (k_{D}) is used along with the relative velocity (between fluid and solid) to quantify the viscous stress between them.

In acoustics, the Stokes law (Cheng, 2012) states how attenuation of a soundwave in free water depends on water viscosity and wave frequency. Scholars in that field have observed that fluid viscosity at high frequency is not identical to that at low frequency, which however is not a severe problem for rock physicists. The reason is that any variation in fluid viscosity in rock physics can be attributed to permeability due to the aforementioned relationship between fluid viscosity and rock permeability. Moreover, attenuation due to the Stokes law in free water (Dziewonski & Anderson, 1981) is far less than attenuation observed in fluid-saturated rocks and is therefore unimportant.

Biot (1956a, 1956b) developed a single porosity theory yielding two kinds of compressional (P) waves in a fluid-saturated rock. The dilatational wave of the first kind was a fast P wave having high velocity and low attenuation. The dilatational wave of the second kind was a slow P wave having low velocity and large attenuation; the wave was characterized by diffusive fluid pressure that drove groundwater seepage while the skeleton was almost static. Biot's theory was more accurate than the storativity equation used for describing fluid pressure transmission in hydrogeology (Domenico & Schwartz, 1997; Li et al., 2020). However, Biot (1956a) severely underestimated velocity and attenuation of ultrasonic P- and shear (S) waves (Jones & Nur, 1983; Li, 2020a; Mochizuki, 1982), although Gassmann (1951) velocity is obtained at low frequency.

The actual rocks may be saturated with two fluids (water and gas), rather than water alone; such rocks are called partially saturated. As gas has much higher compressibility and much lower viscosity than water, the physical properties of water plus gas are distinctively different from those of a single liquid. White (1975) developed a pocket model of three phases (skeleton, water and gas). By deriving the bulk modulus as a function of frequency and saturation using the Lagrangian approach, he obtained the velocity and the quality factor of the P wave as a function of frequency and saturation, respectively. In his model, shear modulus was kept unchanged, as the shear modulus of a rock would not be affected by fluids. Consequently, there was neither velocity dispersion nor attenuation for the S wave in his model, which, however, was inconsistent with laboratory observations (Toksöz et al., 1979). Also, his conceptual model was challenged by the fact that gas would rise by the buoyancy force such that after long geologic periods, gas would not coexist with water inside pores.

Dvorkin et al. (1995) constructed a BISQ (Biot squirt) model based on the squirt between microcracks and pores. The mechanism was reasonable for a P wave because microcracks are indeed more compliant to pressure than pores. However, their model suffered from the question whether such a squirt exists for an S wave (Li, 2020a, 2020b).

Pride and Berryman (2003a, 2003b) proposed a double permeability model to simulate P and S waves in fluid-saturated rock, based on the squirt mechanism in Dvorkin et al. (1995). However, the compressibility matrices representing the constitutional relations (Pride & Berryman, 2003a, 2003b; Pride et al., 2004) were set to be symmetric and, consequently, their model had difficulty in yielding the Gassmann (1951) velocity at the low frequency limit. It is not difficult to show that the compressibility matrices (Pride & Berryman, 2003a, 2003b; Pride et al., 2004) are indeed asymmetric and their symmetric compressibility matrices were inaccurate. Notably, Li et al. (2021) used unsymmetric

compressibility matrices to successfully yield the Gassmann (1951) velocity at the low frequency limit.

When simulating S wave attenuation, Pride and Berryman (2003a, 2003b) and Pride et al. (2004) adopted the squirt mechanism from BISQ (Dvorkin et al., 1995). In contrast, based on the Stokes second problem (Schlichting, 1968), Li (2020a, 2020b) developed a single porosity model of an S wave which effectively predicted velocity and attenuation in Berea and Boise sandstone. The idea was that with increasing frequency, the fluid velocity profile in pores will have a thinning boundary layer which significantly increases the viscous stress (between solid and fluid) and decreases permeability (Johnson et al., 1987). At low frequency, the velocity profile of fluid flow in pores is parabolic and the Stokes boundary layer has a thickness of about the pore radius. As the frequency increases, high-frequency oscillations will appear on the profile, causing a thinner Stokes boundary layer (Schlichting, 1968). As the boundary layer becomes thinner, the viscous stress will increase and permeability will decrease. Nonetheless, the modeling by Li (2020b) on ultrasonic velocity and attenuation in Berea sandstone yielded inconsistent permeability values. This may be attributable to be the problem of single porosity. In this regard, a double porosity model should be superior.

As mentioned above, in Darcy's law, permeability is invariably related to fluid viscosity. Petroleum engineers have defined mobility as the ratio between permeability and fluid viscosity to describe how fluid pressure drives fluid flow. Batzle et al. (2006) were the first to recognize that for rocks with low permeability saturated with high-viscosity fluid (low mobility), strong dispersion and attenuation will shift into the seismic band, while for high-mobility fluid, they will remain at sonic or ultrasonic bands. Their laboratory technique was called the forced oscillation method (FOM), in which Young's modulus and the corresponding uniaxial attenuation at seismic frequency were measured.

Using the FOM, Mikhaltsevitch et al. (2014) measured the quality factor (Q_E) in highly permeable sandstones saturated with water as about 1000 in a frequency range of 0.1–100 Hz, which was consistent with the consensus of small attenuation at low frequency. For low-permeability sandstones, Q_E was measured to be 25–30, suggesting that low permeability causes the peak attenuation and the associated characteristic frequency (ω_C) to shift to low frequency. In contrast, our dimensional analysis of Biot's (1956a) theory reveals that with decreasing permeability, the peak attenuation and ω_C will shift toward the high-frequency end. Therefore, the experimental results in Mikhaltsevitch et al. (2014) confirmed that the wavelength-scale attenuation (Biot, 1956a, 1956b) is not the dominant mechanism of P-wave attenuation. However, whether an S wave has the same trend as a P wave remains unclear.

Besides decreasing permeability, another way to cause the peak attenuation and ω_C shift to low frequency (thus observable by FOM) is by increasing fluid viscosity. Subramaniyan et al. (2015) used glycerin and a low-permeability Fontainebleau sandstone in their FOM experiments to observe the change of attenuation with frequency. They found that ω_C occurred at 6 Hz. Chapman et al. (2019) conducted a similar experiment on highly permeable Berea sandstone, but did not observe any peak attenuation in the frequency range of 1–10 Hz because high permeability tends to shift the peak attenuation to a higher frequency.

The above FOM used a cylindrical bar to investigate Young's modulus, and thus is unsuitable for the study of S waves. For this reason, in this paper we use the results from ultrasonic experiments. At ultrasonic frequency, the time scale is very short and fluid acceleration is important. In Sect. 2, we investigate a novel reverse squirt (in the throat) as a side effect caused by fluid acceleration. In Sect. 3, a double porosity model based on the mechanism is constructed. In Sect. 4, the model is shown to be very successful in predicting the phase velocity (V_s) and quality factor of S waves (Q_s) ultrasonically measured in two sandstone samples. The paper concludes with the Discussion.

2. *Reverse Squirt Due to Fluid Acceleration*

Pores have fluid inside, but fluids have zero shear modulus. For this reason, the shear modulus of pores vanishes. For the bulk modulus of an undrained pore,

Gassmann (1951) and Walsh (1965) showed that a change in the confining pressure is invariably associated with a change in fluid pressure. In other words, as long as the confining pressure is fixed, the fluid pressure, the fluid density and the pore volume do not change. Because an S wave by definition does not change the confining pressure, neither the pore volume nor the fluid pressure will change for an undrained pore. Nonetheless, for several pores between which fluid can drain, fluid pressure may be different; the heterogeneous distribution of pore pressure may invalidate the Gassmann (1951) equation (Zhao et al., 2020, 2021).

As depicted in Fig. 1, main pore A has a front wall (A+) and a back wall (A−). As a solid accelerates, the front wall (A+) has a pulling action on the fluid (where a negative pressure is generated) while the back wall (A−) has a pushing action on the fluid (where a positive pressure is generated). If the main pores are completely sealed/undrained, the pressure difference inside A or B will drive fluid to accelerate and forces the fluid to have the same acceleration/velocity as the solid. However, as a periodic neighbor of A, main pore B also has a negative pressure on its front wall (B+) and a positive pressure on its back wall (B−). As such, a pressure difference automatically arises between A− and B+. The positive pressure on A− will drive fluid in the throat to squirt toward the negative pressure on B+. The squirt in the throat has a flow direction opposite to the direction of fluid acceleration in main pores A and B. Reverse squirt refers to flow in a throat driven by the pressure difference due to fluid acceleration in the main pores. During this process, shear stress does not change the average fluid pressure in pores.

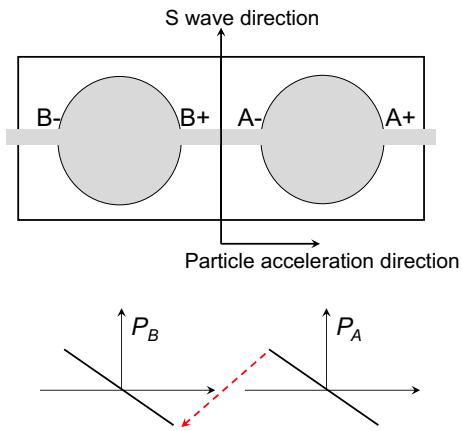

Figure 1
A schematic reverse squirt due to fluid acceleration. As a solid accelerates toward the right-hand side, there is a pressure difference inside the main pores (A and B) which automatically forms a pressure difference in the connecting throat (between A− and B+, represented by the red dashed line). This pressure difference drives a squirt (toward the left-hand side) in the throat whose direction is opposite to the direction of acceleration. Note that fluid is represented in gray; P_A and P_B are fluid pressure in A and B, respectively

3. Model of the S Wave

3.1. Equations from Physics

In Fig. 2, neither the main pore nor the throat has any changes in its spatial volume, because an S wave can only change the shape of the pore and throat, and not their volumes (which is the distinct difference between S waves and P waves). Fluid motion in the space of the main pore and throat is a boundary value problem of viscous flow.

An S wave is supposed to propagate in the y direction, while the Lagrangian motion is in the x

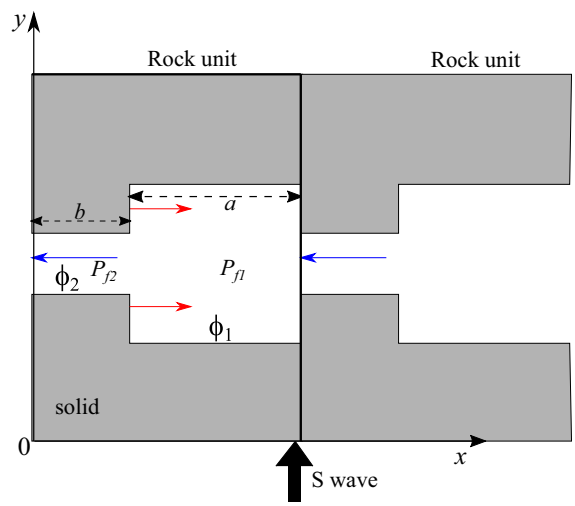

Figure 2
Double porosity model in which there is a reverse squirt (blue arrow) due to acceleration (red arrow). The pressure difference between the two main pores drives a reverse squirt in the throat. The rock unit (bounded by the x and y axes and two black bold lines) is periodic along the x direction, in which a and b are lengths of the main pore and throat, respectively, ϕ_1 and ϕ_2 are their local porosities, and P_{f1} and P_{f2} are their fluid pressures

direction; t denotes time. Fluid momentum equations in the main pore and throat are

$$-\frac{\mu}{k_1}(q_1-\phi_1 v)=\frac{\partial P_{\mathrm{p1}}}{\partial x}+\frac{\rho_{\mathrm{f}}}{\phi_1}\frac{\partial q_1}{\partial t}, \tag{1}$$

$$-\frac{\mu}{k_2}(q_2-\phi_2 v)=\frac{\partial P_{\mathrm{p2}}}{\partial x}+\frac{\rho_{\mathrm{f}}}{\phi_2}\frac{\partial q_2}{\partial t}, \tag{2}$$

respectively, where subscripts 1 and 2 denote the main pore and throat, respectively; P_{p}, q and v are fluid pressure, Darcy flux rate and solid velocity, respectively; ϕ_1 and ϕ_2 are local porosities in the main pore and throat, respectively; k_1 and k_2 are local permeabilities in the main pore and throat, respectively; ρ_{f} and μ are fluid density and viscosity, respectively. Essentially, Eqs. (1–2) are Newton's second law applied to fluid in the main pore and throat, respectively. The left-hand sides are viscous stress between solid and fluid, while the right-hand sides are pressure gradient and fluid acceleration. As a reminder, by considering the inertial terms (the second terms on the right-hand sides), Eqs. (1–2) are a generalization of Darcy's law to high frequencies, in which the left-hand sides use a generalized permeability (rather than Darcy permeability) to quantify the viscous stress.

Often, the quantities in a porous medium are in a statically average sense. However, we use the concept of a (representative) rock unit (a fluid–solid aggregate) for an acoustical model at the pore scale. In this way, the inverted parameters are likely to represent the statistically averaged characteristics of a reservoir rock.

Each rock unit consists of a skeleton and fluid, and the macroscopic motion of fluid along the x direction is the same. From a rock unit to its neighboring units in the x direction, macroscopic pressure is the same, but the pressure within a single rock unit can vary. In other words, the macroscopic gradient of fluid pressure in the x direction vanishes, but the microscopic gradient is not zero, which yields a periodic condition of fluid pressure as follows.

$$b\frac{\partial P_{\mathrm{p2}}}{\partial x}+a\frac{\partial P_{\mathrm{p1}}}{\partial x}=0, \tag{3}$$

where a and b are the lengths of the main pore and throat, respectively. Substituting Eqs. (1–2) into Eq. (3) yields the momentum equation of fluid as follows.

$$\begin{aligned}&-\frac{a\mu}{k_1}(q_1-\phi_1 v)-\frac{b\mu}{k_2}(q_2-\phi_2 v)\\&=\frac{a\rho_{\mathrm{f}}}{\phi_1}\frac{\partial q_1}{\partial t}+\frac{b\rho_{\mathrm{f}}}{\phi_2}\frac{\partial q_2}{\partial t}.\end{aligned} \tag{4}$$

Essentially, the momentum equation of a rock unit is Newton's second law applied to the whole unit, i.e.,

$$G\frac{\partial^2 u}{\partial y^2}=\rho_{\mathrm{s}}\frac{\partial^2 u}{\partial t^2}+\rho_{\mathrm{f}}\frac{a}{a+b}\frac{\partial q_1}{\partial t}+\rho_{\mathrm{f}}\frac{b}{a+b}\frac{\partial q_2}{\partial t}, \tag{5}$$

where u, ρ_{s} and G are shear displacement, density and shear modulus of the skeleton, respectively.

Because of fluid mass conservation, the relative water flux must be continuous between the main pore and throat, i.e.,

$$q_1-v\phi_1=q_2-v\phi_2. \tag{6}$$

Equations (4–6) are three equations involving three independent unknowns, i.e., u, q_1 and q_2; note that v is dependent on u as $v=\frac{\partial u}{\partial t}$. Once they are solved, P_{p1} and P_{p2} can be obtained via Eqs. (1) and (2), respectively.

One might think that in Fig. 2, the main pore and throat have different length scales such that their wavenumbers (k) should differ from each other. Actually, the spacing length (interval) between two pores is the same as that between two throats, such that k is the same between pore and throat, except that there is a phase difference between their plane waves.

3.2. Wavenumber Equation

Letting $\frac{q_1}{\phi_1}=Q_1(\omega)\mathrm{e}^{i(\omega t-ky)}$, $\frac{q_2}{\phi_2}=Q_2(\omega)\mathrm{e}^{i(\omega t-ky)}$, $v=V(\omega)\mathrm{e}^{i(\omega t-ky)}$, we get $u=\frac{V(\omega)}{i\omega}\mathrm{e}^{i(\omega t-ky)}$. With these relations, Eqs. (4–6) are in the frequency domain as follows.

$$\begin{aligned}&-\frac{a\mu\phi_1}{k_1}(Q_1-V)-\frac{b\mu\phi_2}{k_2}(Q_2-V)\\&=\rho_f(aQ_1+bQ_2)\omega i,\end{aligned} \tag{7}$$

$$GVk^2 = \omega^2\left(\rho_S V + \rho_f \frac{a\phi_1}{a+b} Q_1 + \rho_f \frac{b\phi_2}{a+b} Q_2\right), \tag{8}$$

$$\phi_1(Q_1 - V) = \phi_2(Q_2 - V), \tag{9}$$

respectively.

Letting $R = \phi_1(Q_1 - V) = \phi_2(Q_2 - V)$ according to Eq. (9), then Eqs. (7–8) become

$$-\mu\left(\frac{a}{k_1} + \frac{b}{k_2}\right)R = \rho_f\left[(a+b)V + \frac{a}{\phi_1}R + \frac{b}{\phi_2}R\right]\omega i, \tag{10}$$

$$GVk^2 = \omega^2(\rho V + \rho_f R), \tag{11}$$

respectively, where $\rho = \rho_s + \phi\rho_f$ denotes the total density.

Solving Eqs. (10–11) yields a wavenumber equation as follows.

$$\frac{k^2 c_s^2}{\omega^2} = 1 - \frac{\frac{\rho_f}{\rho}}{\left(\frac{a}{\phi_1} + \frac{b}{\phi_2}\right)\frac{1}{a+b} - i\frac{\mu}{\rho_f\omega}\left(\frac{a}{k_1} + \frac{b}{k_2}\right)\frac{1}{a+b}}, \tag{12}$$

where $c_s = \sqrt{\frac{G}{\rho}}$ is the S-wave velocity in undrained rock.

The wavenumber equation in physics is the eigenvalue equation in the mathematical sense. In other words, Eq. (12) has a general meaning, independent of 1D, 2D or 3D.

3.3. The Limits of Low and High Frequency

At the low-frequency limit ($\omega \to 0$), Eq. (12) degenerates to

$$c_s^2 \frac{k^2}{\omega^2} \to 1, \tag{13}$$

meaning that S-wave velocity at low frequency tends to the undrained velocity (c_s). If there are no throats, i.e., $\phi_2 = 0$, then Eq. (12) will reduce to (13).

As $\omega \to +\infty$, Eq. (12) degenerates to

$$c_s^2 \frac{k^2}{\omega^2} \to 1 - \frac{\frac{\rho_f}{\rho}}{\left(\frac{a}{\phi_1} + \frac{b}{\phi_2}\right)\frac{1}{a+b}}. \tag{14}$$

Given that the right-hand side of Eq. (14) is always smaller than unity, the S-wave velocity ($\frac{\omega}{k}$) at the high-frequency limit is invariably higher than the undrained velocity (c_s).

3.4. Phase Velocity and the Quality Factor

Equation (12) is solved as follows.

$$\frac{kc_E}{\omega} = \sqrt{1 - \frac{\frac{\rho_f}{\rho}\left(\frac{a}{\phi_1} + \frac{b}{\phi_2}\right)\frac{1}{a+b}}{\left[\left(\frac{a}{\phi_1} + \frac{b}{\phi_2}\right)\frac{1}{a+b}\right]^2 + \left[\frac{\mu}{\rho_f\omega}\left(\frac{a}{k_1} + \frac{b}{k_2}\right)\frac{1}{a+b}\right]^2} - i\frac{\frac{\mu}{\rho\omega}\left(\frac{a}{k_1} + \frac{b}{k_2}\right)\frac{1}{a+b}}{\left[\left(\frac{a}{\phi_1} + \frac{b}{\phi_2}\right)\frac{1}{a+b}\right]^2 + \left[\frac{\mu}{\rho_f\omega}\left(\frac{a}{k_1} + \frac{b}{k_2}\right)\frac{1}{a+b}\right]^2}} = \sqrt{A - iB}, \tag{15}$$

where A and $-B$ are the real and imaginary parts inside the square root.

Phase velocity (V_s) and the quality factor (Q_s) are as follows; please refer to Li (2020a).

$$\frac{V_s}{c_s} = \frac{1}{\left(\frac{\sqrt{A^2+B^2}+A}{2}\right)^{\frac{1}{2}}}, \tag{16}$$

$$Q_s = \frac{1}{2}\left(\frac{\sqrt{A^2+B^2}+A}{\sqrt{A^2+B^2}-A}\right)^{1/2}. \tag{17}$$

3.5. Some Constraints

Referring to Fig. 2, the first and second porosities are $\frac{a\phi_1}{a+b}$ and $\frac{b\phi_2}{a+b}$, respectively. Thus, the total porosity (ϕ) is as follows:

$$\phi = \frac{a\phi_1}{a+b} + \frac{b\phi_2}{a+b}. \tag{18}$$

As depicted in Fig. 2, the main pore by definition has local porosity (ϕ_1) invariably much higher than that of the throat (ϕ_2). This puts a constraint in our program, i.e.,

$$\phi_1 \geq 2\phi_2. \tag{19}$$

Consider Darcy seepage along the x direction, in which case the throat permeability,$k_2(\omega = 0)$, is dominant in Darcy permeability (k_D). The main pore permeability, $k_1(\omega = 0)$, is unimportant. It is not difficult to show that

$$\frac{k_2(\omega = 0)}{k_D} = \frac{b}{a+b}. \tag{20}$$

For the main pore fluid, the pressure difference originates from the pushing and sucking forces caused by the back and front walls of the main pore, respectively (Fig. 1). This pressure difference in the main pore is roughly balanced with the acceleration of fluid inside. Shear stress caused by the lateral/horizontal wall on the main pore fluid can be neglected, which can be realized by setting $k_1(\omega)$ to a large value. Note that if the main pore is infinitely long, $k_1(\omega)$ cannot be neglected because the Stokes boundary layer is very sharp at high frequency (Li, 2020a). However, in our double porosity model (Fig. 2), the pressure difference caused by the back/pushing and front/sucking walls is the major force for the acceleration of fluid in the main pores, and the Stokes boundary layer associated with $k_1(\omega)$(Li, 2020a) is unimportant (shear stress on the main pore fluid by the lateral/horizontal wall is unimportant).

4. Illustrative Examples

4.1. Berea Sandstone

Berea sandstone is a classic sedimentary rock which formed in the Upper Devonian Period. It is fine-grained, and the grains are angular rather than rounded, because the traveling distance was not long and the erosion by surface streams was not strong. Over the last few decades, Berea sandstone has been used extensively in the petroleum industry to represent conventional oil/gas reservoirs because of its homogeneity and isotropy.

The measured parameters of Berea sandstone are listed in Table 1. Similar to Li (2020b), using the total porosity of 0.23 (Øren & Bakke, 2003) improves the fitting slightly better than using an effective porosity of 0.19 (Wang, 2000). Attenuation (Q^{-1}) arises from a variety of mechanisms such as flow of viscous fluid (Jaeger et al., 2007), internal friction in dry rocks (Ricker, 1977), or Rayleigh scattering by grains (Blair, 1990). The total attenuation is larger than attenuation induced by viscous fluid flow alone, and accordingly the total quality factor is invariably lower than the quality factor (Q_s) induced by viscous fluid flow alone. According to Toksöz et al. (1979) and Li (2020b), Q_s was measured at a receiving frequency of 0.5 MHz as 13.7 for brine-saturated Berea sandstone. The velocity was measured at this frequency as 2220 m/s (Toksöz et al., 1979).

We set the length ratio of the throat as $\frac{b}{a+b} = 0.1$, $\phi_2 = 0.5\phi$ (the second porosity is 0.0115). The local static permeability of the throat is $k_2(\omega = 0) = \frac{b}{a+b}k_D$ according to Eq. (20). As introduced earlier, the Stokes boundary layer at high frequency tends to decrease the static permeability, and so we set the

Table 1

Measured parameters of Berea sandstone and brine

Parameters	Value	Unit	References
Density of skeleton, ρ_s	2110	kg m^{-3}	Measured by authors
S-wave velocity of skeleton, c_{s0}	2320	m s^{-1}	Toksöz et al. (1979)
Porosity, ϕ	0.23		Øren and Bakke (2003)
Darcy permeability, k_D	0.075×10^{-12}	m^2	Toksöz et al. (1979)
Density of brine, ρ_f	1067	kg m^{-3}	Toksöz et al. (1979)
Viscosity of brine, μ	0.001	Pa s	Kundu (1990)

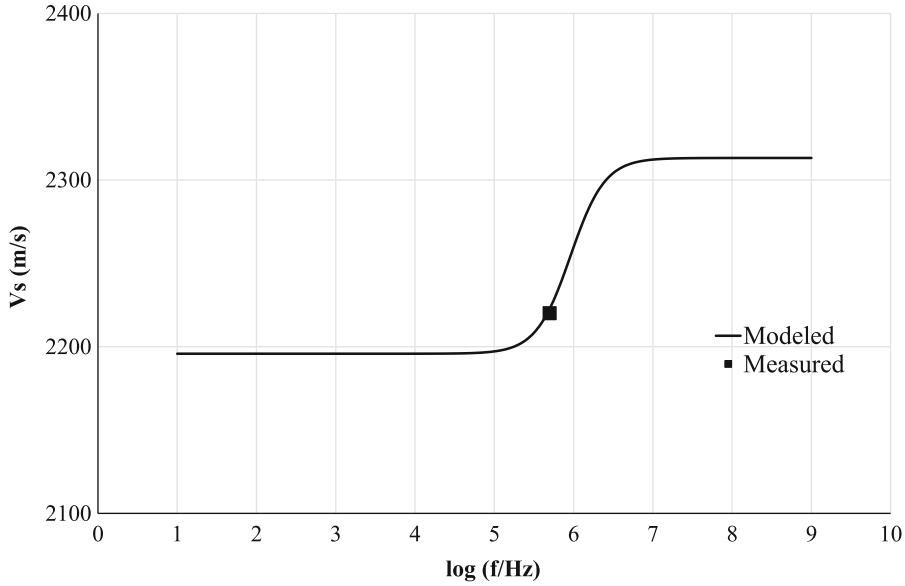

Figure 3
Modeled velocity (V_s) versus the ultrasonic measurement (square) of an S wave in Berea sandstone, in which f is frequency. The length ratio of throat $b/(a + b) = 0.1$; the local porosity of throat $\phi_2 = 0.115$; throat permeability $k_2 = 0.5k_D b/(a + b)$ where k_D, a and b are the Darcy permeability, main pore length and throat length, respectively

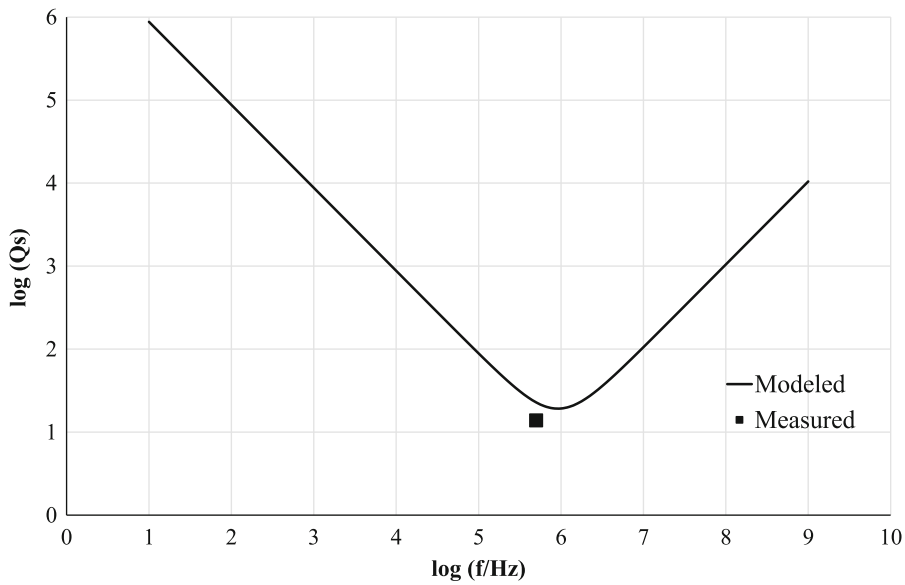

Figure 4
Modeled quality factor (Q_s) versus the ultrasonic measurement (square) of an S wave in Berea sandstone, in which f is frequency. The length ratio of the throat $b/(a + b) = 0.1$; the local porosity of the throat $\phi_2 = 0.115$; permeability in the throat is $k_2 = 0.5k_D b/(a + b)$ where k_D, a and b are the Darcy permeability, main pore length and throat length, respectively. Note the square is the quality factor induced by viscous flow alone

Table 2

Measured parameters of Boise sandstone and water

Parameters	Value	Unit	References
Density of skeleton, ρ_s	1940	kg m^{-3}	Gregory (1976)
S-wave velocity of skeleton, c_{s0}	2090	m s^{-1}	Gregory (1976)
Porosity, ϕ	0.268		Gregory (1976)
Darcy permeability, k_D	10^{-12}	m^2	Gregory (1976)
Density of water, ρ_f	1000	kg m^{-3}	Kundu (1990)
Viscosity of water, μ	0.001	Pa s	Kundu (1990)

high-frequency permeability of the throat to half of the static permeability, i.e., $k_2 = 0.5k_2(\omega = 0)$. Eventually, our double porosity model yields V_s of 2223 m/s and Q_s of 22.8 at 0.5 MHz; see Figs. 3 and 4, respectively. The predicted V_s is very close to the measured value, and the predicted Q_s also agrees very well with the measured value. This modeling is called the benchmark of Berea sandstone. Overall, the modeling on Berea sandstone is superior to that in Li (2020b). The determined parameters are very reasonable, in that the length ratio of the throat is very short and the second porosity is only 5% of the total porosity.

With $\frac{b}{a+b} = 0.1$, $\phi_2 = 0.1\phi$ (the second porosity is 0.0023) and $k_2 = 0.4k_2(\omega = 0)$, the model yields V_s of 2220 m/s and Q_s of 35.0 at 0.5 MHz. The velocity is very good between the model and measurement. The second porosity is unreasonably low, and the modeled Q_s does not agree with the measured value.

With $\frac{b}{a+b} = 0.5$, $\phi_2 = 0.5\phi$ (the second porosity is 0.0575), the model at best yields V_s of 2247 m/s and Q_s of 24.7 at 1 MHz. The modeled values are not as good as the above benchmark. This is because the second porosity is unreasonably high.

With $\frac{b}{a+b} = 0.9$, $\phi_2 = 0.5\phi$ (the second porosity is 0.1035), the model yields Q_s far away from the

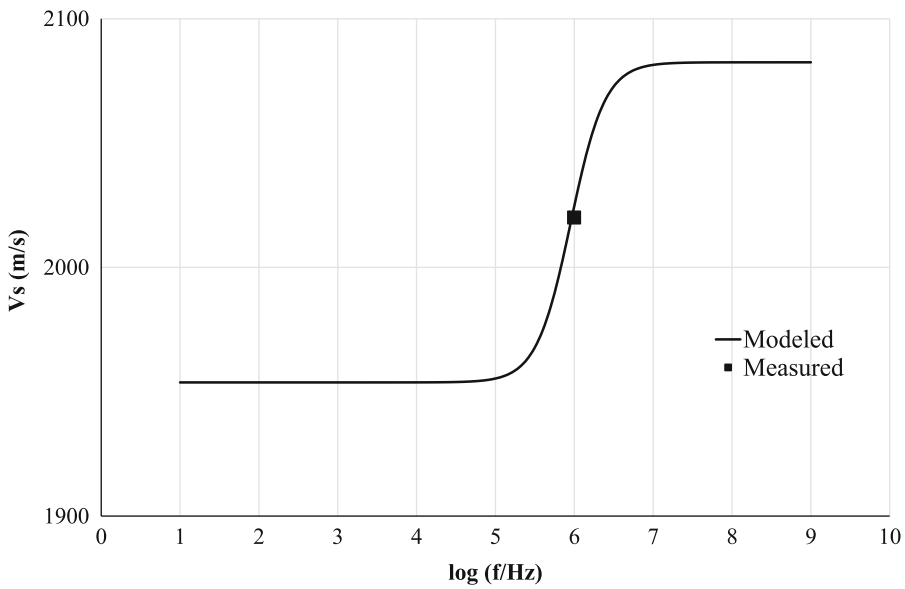

Figure 5

Modeled velocity (V_s) against the ultrasonic measurement (square) of an S wave in Boise sandstone, in which f is frequency. The length ratio of the throat $b/(a + b) = 0.1$; the local porosity of the throat $\phi_2 = 0.14$; permeability in the throat $k_2 = 0.05k_D b/(a + b)$ where k_D, a and b are the Darcy permeability, main pore length and throat length, respectively

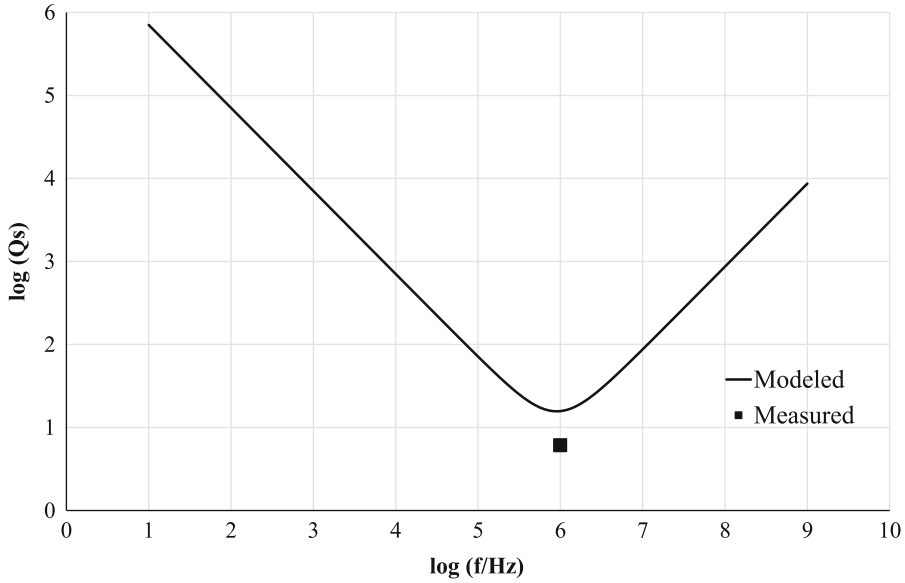

Figure 6
Modeled quality factor (Q_s) against the ultrasonic measurement (square) of an S wave in Boise sandstone, in which f is frequency. The length ratio of the throat $b/(a + b) = 0.1$; the local porosity of the throat $\phi_2 = 0.14$; permeability in the throat $k_2 = 0.05k_D b/(a + b)$ where k_D, a and b are the Darcy permeability, main pore length and throat length, respectively. Note the square is the total quality factor which is invariably lower than the quality factor induced by viscous flow alone

measured value. This is because both the length ratio of the throat and the second porosity are too high.

4.2. Boise Sandstone

Boise sandstone is a sedimentary rock which formed in the Upper Miocene. The sandstone saturated with water is also used for validating the model. Measured parameters of Boise sandstone are listed in Table 2, in which effective porosity is 0.268 (Gregory, 1976). Using the total porosity of 0.28 slightly improved the fitting. S-wave velocity measured at 1 MHz is 2020 m/s (Gregory, 1976). Toksöz et al. (1979) measured the total attenuation (Q^{-1}) with a receiving frequency of 0.5 MHz as 6.1 for the brine-saturated sandstone.

Ideally, as in the preceding subsection, Q_s (induced by viscous fluid flow alone) should be used on the measurement side. However, as attenuation of the dry rock was not measured, we have to use the total attenuation (Q^{-1}) on the measurement side. Also, although the receiving frequency of 0.5 MHz is usable, the sending frequency of 1 MHz may be more appropriate. In the fitting below, the sending frequency and the total quality factor (Q) are used.

We set $\frac{b}{a+b} = 0.1$ and $\phi_2 = 0.5\phi$ (the second porosity is 0.014). The high-frequency permeability of the throat is set to 5% of the static permeability, i.e., $k_2 = 0.05k_2(\omega = 0)$. Eventually, the model yields V_s of 2025 m/s and Q_s of 15.7 at 1 MHz; the modeling results are depicted in Figs. 5 and 6. The modeled V_s is very close to the measured value, and the modeled Q_s also agrees well with the measured value. Overall, the modeling on Boise sandstone is superior to Li (2020a, 2020b). It is very reasonable that the length ratio of the throat is very short and the second porosity is 5% of the total porosity.

Similar to the first example, we change the length ratio of the throat ($\frac{b}{a+b}$) and the second porosity ($\frac{b\phi_2}{a+b}$); the conclusion achieved by Berea sandstone is also valid for Boise sandstone. In short, if either of these two modeling parameters is unreasonable, the model will yield Q_s inconsistent with the measured value.

5. Discussion

Overall, the above simulations involve two ultrasonically measured quantities (V_s and Q_s) for solving three unknowns ($\frac{b}{a+b}$, $\frac{\phi_2}{\phi}$ and $\frac{k_2}{k_2(\omega=0)}$). As such, the mathematical problem is underdetermined and the inverted solution is non-unique. Nevertheless, it has been shown that appreciable changes in the resulting values of the three parameters cannot yield a good prediction of V_s and Q_s. In this regard, the results represent well a finite space of solution. Further determination of their accurate values would require additional constraints.

According to Eq. (12), the phase velocity and quality factor in our model are dependent on a dimensionless angular frequency (Ω) as follows.

$$\frac{1}{\Omega} = \frac{\mu}{\rho_f \omega}\left(\frac{a}{k_1} + \frac{b}{k_2}\right)\frac{1}{a+b}. \tag{21}$$

A dimensionless number is better than its dimensional counterpart in that it essentially controls how different parameters act in a model. In other words, different configurations of the parametric values as on the right-hand side of (21) may yield the same effect represented by the same dimensionless number as on the left-hand side. Equation (21) predicts that for an S wave, increasing permeability will shift the curves of V_s and Q_s to the low-frequency end, while decreasing permeability will shift the curves to the high-frequency end.

It is interesting to explore why throat permeability in Berea sandstone $k_2 = 0.5k_D\frac{b}{a+b}$, whereas in Boise sandstone, $k_2 = 0.05k_D\frac{b}{a+b}$. A numeric check finds that the throat permeabilities in the two sandstones are actually close to each other. Actually, Berea sandstone is more or less similar to Boise sandstone. The major difference is that the former has much smaller Darcy permeability than the latter.

Berea sandstone is a homogeneous rock, or fissures-free. In contrast, Boise sandstone is inhomogeneous, with wide distribution of grain diameter and having fractures (Cheung et al., 2012). For Berea sandstone, it is matrix that controls both seepage experiments (that are used for the Darcy permeability measurement) and S-wave attenuation. In contrast, for Boise sandstone, it is fractures that largely control Darcy permeability, whereas it is the matrix that controls S-wave attenuation (fractures only play a minor role in S-wave attenuation). In other words, an S wave cannot resolve fractures in Boise sandstone and the use of the associated Darcy permeability measured by seepage experiments is inappropriate for an S wave in Boise sandstone. This problem does not exist for homogeneous Berea sandstone free of fractures.

In contrast to Biot (1956b) who used variable fluid viscosity and constant Darcy permeability to quantify the viscous stress at high frequencies, Johnson et al. (1987) worked out a dynamic (frequency-dependent) permeability. Their dynamic permeability is qualitatively correct in that with the increase of frequency, it will decrease from Darcy permeability to zero. However, it suffered from two disadvantages: (1) their permeability violated the consensus that permeability is used along fluid viscosity and the relative velocity to quantify the viscous stress; (2) the expression of their permeability required specifying several additional unknown parameters.

In the double permeability model (Pride & Berryman, 2003a, 2003b; Pride et al., 2004), squirt associated with an S wave was hypothesized to be driven by the change of the average pore pressure caused by shear stress on the rock unit, irrelevant to accelerated fluid motion. At one moment, their squirt flux was either from fissures into the main pore space or in the reverse. However, shear stress essentially only changes angle or shape, rather than volume. In this regard, the change of the average pore pressure by shear stress on the rock unit should be negligible. In contrast, our squirt associated with an S wave is driven by the pressure difference inside main pores due to the fluid acceleration (the average pore pressure remains unchanged because a shear stress cannot invoke change of pore/throat volume). In contrast to the double permeability model (Pride & Berryman, 2003a, 2003b; Pride et al., 2004) in which their squirt flux was between fissures and the main pore space (fluid mass in fissures was not conserved), fluid in this study essentially flows between pores via a connecting throat (fluid mass in the throat is conserved; Fig. 1).

Pride and Berryman (2003a, 2003b) and Pride et al. (2004) used the far-field approach, i.e., a squirt coefficient along with the pressure difference

between the throat and the main pore space, for quantification of the squirt flux between them. However, in the viewpoint of the near field, the space of the throat is very narrow such that it is very difficult for a net fluid mass to enter a throat from the main pore space. Their squirt coefficient may exaggerate the actual exchange of fluid mass between the throat and the main pore space. In contrast, our model allows pore fluid to enter a throat on one side and to exit the throat on the other side, which in the viewpoint of fluid mass conservation is more realistic than that in their double permeability model.

Dvorkin et al. (1995) posited that squirt was between microcracks and the main pore space. In contrast, Murphy et al. (1986), Pride and Berryman (2003a, 2003b), and Pride et al. (2004) proposed that squirt was between contact of grains and the main pore space. The latter is more reasonable than the former, as there are few microcracks in many sandstones (Murphy et al., 1986).

By analytical continuation, our model predicts Q_s of 10^6 at a frequency of 10 Hz (Figs. 4, 6). Hauksson and Shearer (2006) measured seismic Q_p (the quality factor of a P wave) and Q_s in the southern California crust. At a depth of 1 km (the depth of an aquifer), Q_s appeared to be about 100. The very low Q_s may arise from (1) groundwater that has softened the skeleton of sedimentary rocks after a long period; (2) the interfaces between multiple lithological layers in the vertical direction causing internal reflections and tuning (Waters, 1981). Another possibility is that lateral inhomogeneity due to different geologic blocks causes reflection or scattering on the horizontal plane.

For dry rocks, a shear stress is more difficult to transmit than pressure, and accordingly, Q_p should be higher than Q_s. Waters (1981) showed that Q_p is much higher than Q_s. However, for water-saturated rocks, a seismic P wave may have large-scale squirt similar to pore-scale squirt, while a seismic S wave does not (according to this study, S-wave attenuation due to acceleration is very small at low frequency). This may be why Q_p is smaller than Q_s in Hauksson and Shearer (2006).

It is desirable to have measurements at frequencies other than ultrasonic frequency to validate our model. However, current FOM experiments only yield data sets on a bar and Young's modulus, not designed for an S wave. Sonic logging notoriously yields Q_s with significant fluctuations with depth, and thus is unsuitable for that purpose. This paper is a preliminary report using two sandstones (homogeneous Berea sandstone and less homogeneous Boise sandstone). Carbonate rocks such as limestone are more complicated than sandstones, and studies with more data or more samples to validate this novel mechanism are planned in the near future.

6. Conclusions

Fluid acceleration in a main pore requires a pressure difference within the pore. As a side effect, this will automatically yield a fluid pressure difference in the throat between two neighboring pores, which drives a reverse squirt in the throat. This mechanism was not recognized previously.

Our earlier single porosity model was based on the Stokes boundary layer which was incapable of yielding very consistent permeability for Berea sandstone. The modeling results on Berea sandstone and Boise sandstone show that the double porosity model in this paper yields velocity and attenuation both surprisingly consistent with those ultrasonically measured.

The previous double permeability models by other researchers hypothesized that the average pore pressure was changed by a shear stress, which violated the nature of shear stress only changing shape (rather than volume or pressure). In contrast, our model leaves the average pore pressure unchanged and is thus more reasonable. The previous double permeability models had squirt (fluid mass flux) between fissures and the main pore space (fluid mass in fissures was not conserved). In contrast, our squirt is between pores via their connecting throat (fluid mass in the throat is conserved).

According to Eq. (21), our S-wave model predicts that increasing permeability will shift the curves of V_s and Q_s to the low-frequency end, while decreasing permeability will shift the curves to the high-frequency end (which is consistent with Biot's theory). At first glance, this trend appears to be opposite to the results of FOM measurements, but actually it is not.

This is because FOM experiments measure uniaxial strain roughly representing a P wave.

Acknowledgements

The research was sponsored by the National Natural Science Foundation of China under Grants 42064006 and 41873075. The authors would like to thank sincerely the Editor and two anonymous reviewers for their positive comments and constructive suggestions.

Data Availability

The data yielded from the model are available with https://doi.org/10.6084/m9.figshare.14493768 at https://figshare.com/s/b35b063cf723574c902b.

Declarations

Conflict of interest The authors have no conflicts of interest to declare.

Publisher's Note Springer Nature remains neutral with regard to jurisdictional claims in published maps and institutional affiliations.

References

Batzle, M. L., Han, D. H., & Hofmann, R. (2006). Fluid mobility and frequency-dependent seismic velocity—Direct measurements. *Geophysics, 71*, N1–N9.

Bear, J. (1972). *Dynamics of fluids in porous medium*. Dover.

Biot, M. A. (1956a). Theory of propagation of elastic waves in a fluid-saturated porous solid I. Lower frequency range. *Journal of the Acoustical Society of America, 28*, 168–178.

Biot, M. A. (1956b). Theory of propagation of elastic waves in a fluid-saturated porous solid II. Higher frequency range. *Journal of the Acoustical Society of America, 28*, 179–191.

Blair, D. P. (1990). A direction comparison between vibrational resonance and pulse transmission data for assessment of seismic attenuation in rock. *Geophysics, 55*(1), 55–60.

Chapman, S., Borgomano, J., Yin, H., Fortin, J., & Quintal, B. (2019). Forced oscillation measurements of seismic wave attenuation and stiffness moduli dispersion in glycerine-saturated Berea sandstone. *Geophysical Prospecting, 67*, 956–968.

Cheng, J. C. (2012). *Principles in acoustics*. Science Press of China.

Cheung, C. S., Baud, P., & Wong, T. (2012). Effect of grain size distribution on the development of compaction localization in porous sandstone. *Geophysical Research Letters, 39*, L21302.

Domenico, P. A., & Schwartz, F. W. (1997). *Physical and chemical hydrogeology*. Wiley.

Dvorkin, J., Mavko, G., & Nur, A. (1995). Squirt flow in fully saturated rocks. *Geophysics, 60*(1), 97–107.

Dziewonski, A. M., & Anderson, D. L. (1981). Preliminary reference Earth model. *Physics of the Earth and Planetary Interiors, 25*(4), 297–336.

Gassmann, F. (1951). Uber die Elasticität Poröser Medien [On the elasticity of porous media]. *Vierteljahrsschrift Der Naturforschenden Gesllschaft in Zürich, 96*, 1–23.

Gregory, A. R. (1976). Fluid saturation effects on dynamic elastic properties of sedimentary rocks. *Geophysics, 41*, 895–921.

Hauksson, E., & Shearer, P. M. (2006). Attenuation models (Q_P and Q_S) in three dimensions of the southern California crust: Inferred fluid saturation at seismogenic depths. *Journal of Geophysical Research, 111*, B05302.

Jaeger, J. C., Cook, N., & Zimmerman, R. (2007). *Fundamentals of rock mechanics* (4th ed.). Wiley-Blackwell.

Johnson, D. L., Koplik, J., & Dashen, R. (1987). Theory of dynamic permeability and tortuosity in fluid-saturated porous media. *Journal of Fluid Mechanics, 176*, 379–402.

Jones, T., & Nur, A. (1983). Velocity and attenuation in sandstone at elevated temperatures and pressures. *Geophysical Research Letters, 10*, 140–143.

Kundu, P. K. (1990). *Fluid mechanics*. Academic Press.

Li, G. (2020a). S wave attenuation based on Stokes boundary layer. *Geophysical Prospecting, 68*, 910–917.

Li, G. (2020b). Velocity and attenuation of ultrasonic S-wave in Berea sandstone. *Acta Geodaetica Et Geophysica, 55*, 335–345.

Li, G., Liu, K., & Li, X. (2020). Comparison of fluid pressure wave between Biot theory and storativity equation. *Geofluids*. https://doi.org/10.1155/2020/8820296

Li, G., Mu, Y., & Xie, C. (2021). Unsymmetric compressibility matrix to model P wave attenuation. *Acta Geodaetica Et Geophysica*. https://doi.org/10.1007/s40328-021-00344-6

Mikhaltsevitch, V., Lebedev, M., & Gurevich, B. (2014). A laboratory study of low-frequency wave dispersion and attenuation in water saturated sandstones. *Leading Edge, 33*, 616–622.

Mochizuki, S. (1982). Attenuation in partially saturated rocks. *Journal of Geophysical Research, 87*, 8598–8604.

Murphy, W. F., Winkler, K. W., & Kleinberg, R. L. (1986). Acoustic relaxation in sedimentary rocks: Dependence on grain contacts and fluid saturation. *Geophysics, 51*, 757–766.

Øren, P., & Bakke, S. (2003). Reconstruction of Berea sandstone and pore-scale modelling of wettability effects. *Journal of Petroleum Science and Engineering, 39*, 177–199.

Pride, S. R., & Berryman, J. G. (2003a). Linear dynamics of double porosity and dual-permeability materials I. Governing equations and acoustic attenuation. *Physical Review E, 68*, 036603.

Pride, S. R., & Berryman, J. G. (2003b). Linear dynamics of double porosity and dual-permeability materials II. Fluid transport equations. *Physical Review E, 68*, 036604.

Pride, S. R., Berryman, J. G., & Harris, J. M. (2004). Seismic attenuation due to wave-induced flow. *Journal of Geophysical Research, 109*, B01201. https://doi.org/10.1029/2003JB002639

Ricker, N. (1977). *Transient waves in visco-elastic media*. Elsevier.

Schlichting, H. (1968). *Boundary layer theory* (6th ed.). Springer.

Subramaniyan, S., Quintal, B., Madonna, C., & Saenger, E. (2015). Laboratory-based seismic attenuation in Fontainebleau sandstone: Evidence of squirt flow. *Journal of Geophysical Research, 120*, 7526–7535.

Toksöz, M. N., Johnston, D. H., & Timur, A. (1979). Attenuation of seismic waves in dry and saturated rocks I. Laboratory Measurements. *Geophysics, 44*(4), 681–690.

Walsh, J. B. (1965). The effect of cracks on the compressibility of rock. *J. Geophy. Res., 70*(2), 381–389.

Wang, H. F. (2000). *Theory of linear poroelasticity—With applications to geomechanics and hydrogeology*. Princeton University Press.

Waters, K. H. (1981). *Reflection seismology—a tool for energy resource exploration*. Wiley.

White, J. E. (1975). Computed seismic speeds and attenuation in rocks with partial gas saturation. *Geophysics*, *40*, 224–232.

Zhao, L., Cao, C., Yao, Q., Wang, Y., Li, H., Yuan, H., Geng, J., & Han, D. (2020). Gassmann consistency for different inclusion-based effective medium theories: Implications for elastic interactions and poroelasticity. *Journal of Geophysical Research, 125*(3), e2019JB018328.

Zhao, L., Wang, Y., Yao, Q., Geng, J., Li, H., Yuan, H., & Han, D. (2021). Extended Gassmann equation with dynamic volumetric strain: Modeling wave dispersion and attenuation of heterogeneous porous rocks. *Geophysics, 86*(3), 149–164.

(Received September 6, 2021, revised February 15, 2022, accepted February 17, 2022, Published online March 14, 2022)